HHS Public Access

Author manuscript

Phys Med Biol. Author manuscript; available in PMC 2017 August 21.

Published in final edited form as:

Phys Med Biol. 2016 August 21; 61(16): 5993–6010. doi:10.1088/0031-9155/61/16/5993.

Dose enhancement effects to the nucleus and mitochondria from gold nanoparticles in the cytosol

AL McNamara[1,2], **WW-Y Kam**[3,4,5], **N Scales**[3], **SJ McMahon**[1,6], **JW Bennett**[3], **HL Byrne**[2], **J Schuemann**[1], **H Paganetti**[1], **R Banati**[3,4,7], and **Z Kuncic**[2]

AL McNamara: amcnamara2@mgh.harvard.edu

[1]Department of Radiation Oncology, Massachusetts General Hospital, Harvard Medical School, 30 Fruit St, Boston, MA 02114, USA [2]School of Physics, University of Sydney, NSW, Australia [3]Australian Nuclear Science and Technology Organisation, Lucas Heights, NSW, Australia [4]Medical Radiation Sciences, Faculty of Health Sciences, University of Sydney, Cumberland, Sydney, New South Wales 2141, Australia [5]Department of Health Technology and Informatics, Hong Kong Polytechnic University, Hung Hom, Hong Kong, China [6]Centre for Cancer Research and Cell Biology, Queen's University Belfast, Belfast, Northern Ireland [7]National Imaging Facility at Brain and Mind Research Institute (BMRI), University of Sydney, Camperdown, Sydney, New South Wales 2050, Australia

Abstract

Gold nanoparticles (GNPs) have shown potential as dose enhancers for radiation therapy. Since damage to the genome affects the viability of a cell, it is generally assumed that GNPs have to localise within the cell nucleus. In practice, however, GNPs tend to localise in the cytoplasm yet still appear to have a dose enhancing effect on the cell. Whether this effect can be attributed to stress-induced biological mechanisms or to physical damage to extra-nuclear cellular targets is still unclear. There is however growing evidence to suggest that the cellular response to radiation can also be influenced by indirect processes induced when the nucleus is not directly targeted by radiation. The mitochondrion in particular may be an effective extra-nuclear radiation target given its many important functional roles in the cell. To more accurately predict the physical effect of radiation within different cell organelles, we measured the full chemical composition of a whole human lymphocytic JURKAT cell as well as two separate organelles; the cell nucleus and the mitochondrion. The experimental measurements found that all three biological materials had similar ionisation energies ~ 70 eV, substantially lower than that of liquid water ~ 78 eV. Monte Carlo simulations for 10 – 50 keV incident photons showed higher energy deposition and ionisation numbers in the cell and organelle materials compared to liquid water. Adding a 1% mass fraction of gold to each material increased the energy deposition by a factor of ~ 1.8 when averaged over all incident photon energies. Simulations of a realistic compartmentalised cell show that the presence of gold in the cytosol increases the energy deposition in the mitochondrial volume more than within the nuclear volume. We find this is due to sub-micron delocalisation of energy by photoelectrons, making the mitochondria a potentially viable indirect radiation target for GNPs that localise to the cytosol.

PACS numbers: 87.14.Gg, 87.15.Aa, 87.16.-b,87.16.Tb,87.52.-g,87.66.Jj

1. Introduction

Due to their high energy absorption coefficient, high density and bio-compatibility, gold nanoparticles (GNPs) have been proposed as radiation dose enhancers in tumour cells (Hainfeld et al. 2004). X-ray irradiated GNPs can enhance radiation damage on sub-microscopic scales by producing an abundance of short-range electrons (< 1 μm) through Auger cascades, without notably altering the dose measured macroscopically (McMahon et al. 2011*a*, McMahon et al. 2011*b*). The short-range effect of GNPs emphasises the importance of sub-cellular uptake and localisation. Since cell death from ionising radiation is generally initiated by damage to the DNA molecule, it is assumed that GNPs need to be placed within the cell nucleus to destroy cancer cells. Experimental studies, however, have shown that GNPs tend to uptake in the cytoplasm of the cell (Peckys & de Jonge 2011, Chithrani et al. 2006) and yet still have a dose enhancing effect (Chithrani et al. 2010). Whether this can be attributed in part to a stress-induced biological mechanism or to physical processes such as radiation damage to extra-nuclear targets is still not known (Taggart et al. 2014) and is the subject of this study.

Growing experimental evidence suggests that the mitochondrion may be a particularly important radiation target outside the nucleus (Murphy et al. 2005, Larsen et al. 2005, Prithivirajsingh et al. 2004, Kam & Banati 2013, Kam et al. 2013, Zhang et al. 2014, Taggart et al. 2014). This is perhaps not surprising given the important functional roles attributed to mitochondria i.e. energy metabolism, apoptosis regulation, reactive oxygen species production, cell signalling (Joza et al. 2001, Raimundo 2014, McBride et al. 2006). Furthermore, α particle microbeam studies where only the cytoplasm of the cell is irradiated, demonstrate that mitochondria are subject to significant radiation damage (Zhang et al. 2013). More notably, cells with an irradiated cytoplasm show significantly more damage to the nucleus when the mitochondrial function is switched off (Zhang et al. 2014), suggesting a complex interplay between mitochondria and the nucleus. A microbeam cell irradiation *in silico* study (Byrne et al. 2015) modelling targeted cytoplasm irradiation showed that while some stray ions may interact with the nucleus, this effect is negligible. Interestingly, this simulation study, as well as others (e.g. Kuncic 2015), showed the importance of dose delocalisation due to Compton scatter and photoelectron ejection (i.e., secondary electrons moving from one part of the cell to another).

These Monte Carlo simulation studies did not, however, investigate dose delocalisation caused by radiosensitive nanoparticles. We address this here using a cell model with small amounts of gold added to different targets (cytosol, nucleus and mitochondria). To accurately model the physical interaction processes on sub-cellular scales, we use realistic chemical compositions for each of the organelles. In this paper, we measured the elemental composition of a whole JURKAT cell, a human T lymphocyte primarily used in cancer drug and radiation studies (e.g. Cataldi et al. 2009), as well as the isolated JURKAT cell nucleus and mitochondrion. Although data on the composition of cells exist, these are generally only for a small subset of elements (e.g Alard et al. 2009) and for non-human cell lines. Tissue compositions (Woodard & White 1986), used for organ dose calculations, are not valid for sub-cellular dose calculations as they only provide averages over the sub-cellular structures

and would include interstitial fluid. Organelle compositions are similarly limited to a small subset of elements across different cell lines (e.g Thiers & Vallee 1957, Nicholls & Chalmers 2004). Having full compositions for cells and their organelles is important for Monte Carlo dose distribution modelling. Currently, most simulation studies use a liquid water medium for modelling tissue, cells and even molecules. Water may be a valid approximation for macro-scale dose calculations in tissue but is not sufficient to capture the full effect of radiation damage at the sub-cellular level (e.g. Champion et al. 2015). Using Monte Carlo simulations, we determine the energy deposition and number of ionisations generated in each different organelle material when irradiated by keV x-rays. We also investigate potential dose enhancement effects from GNPs in a realistic composition by adding gold to each different material. Simulations were also performed to investigate the effect on the nucleus and mitochondrion when gold is present in the cytosol.

2. Methods

The elemental composition of a whole JURKAT cell as well as two separate organelles, the cell nucleus and mitochondria, were determined using three different experimental analysis techniques: Carbon Hydrogen Nitrogen Sulphur (CHNS) analysis, inductively coupled plasma mass spectrometry (ICP-MS) and neutron activation analysis (NAA). The data extracted from the experimental analyses were used to develop a Monte Carlo simulation of a cell to investigate the energy deposition and total number of ionisation events occurring in the different biological compositions, in both the presence and absence of trace amounts of gold.

2.1. Experimental methodology

Cell culture and organelle extraction—JURKAT cells between passages 6 to 12 were used in the experiment. Cells were seeded at a density of 5×10^5 cells/ml and maintained at 37°C with 5% CO_2 in DMEM (Dulbecco's Modified Eagle Medium) supplemented with 10% FBS (Foetal Bovine Serum), 2 mML glutamine, 100 units/ml penicillin and 100 μg/ml streptomycin. Confluent culture from 20 flasks (T75 flask) were pooled together, washed by DPBS (Dulbecco's phosphate-buffered saline) and pelleted by centrifugation. Supernatant was removed and the whole cell pellet was either snap frozen in liquid nitrogen or immediately used for organelle extraction.

The cell nucleus and mitochondria were isolated separately, to reduce the possibility of cross contamination. The whole cell pellet was used for mitochondrial isolation using the Mitochondria Isolation Kit for profiling cultured cells (Sigma Aldrich, St. Louis, MO, USA). A separate whole cell pellet was prepared for nucleus isolation using the Nuclei EZ prep nuclei isolation kit (Sigma Aldrich, St. Louis, MO, USA). Isolation procedures were performed according to the manufacturer protocols and the isolated organelles were immediately snap frozen.

The frozen whole cell or organelle pellet was immediately used for freeze-drying overnight at 0.011 atm at room temperature using Freeze Dryer Christ Alpha ~ 1–2/LD Plus. A net dry weight of ~ 3 to 5 mg was obtained for each whole cell or organelle pellet. The freeze-dried pellets were stored in a desiccator at room temperature until analysis.

Carbon Hydrogen Nitrogen Sulphur (CHNS) analysis—Freeze-dried whole cell and organelle pellet from three independent preparations were sent to the Chemical Analysis Facility at Macquarie University, Australia for CHNS analysis. The samples were analysed with an Elemental Analyser Model PE2400 CHNS/O (Perkin-Elmer, Shelton, CT, USA) ‡. Oxygen concentrations were not determined since a sample size of 5–10 mg was required.

Inductively coupled plasma mass spectrometry (ICP-MS)—Sample digestion was conducted by vortexing samples at 3000 rpm with 1 mL of Suprapur concentrated nitric acid (Merck) for 45 minutes, quantitatively transferring and then making up a total volume of 5 mL with additional Suprapur nitric acid. A blank sample was also carried through this procedure. Samples were then analysed as a dilution set to account for variability in concentration of different elements. A set of samples diluted by a factor of 20, 100, 1000 and 5000 was used.

Samples were analysed with a Bruker (formerly Varian) 820-MS ICP-MS instrument fitted with a Micromist® concentric glass nebuliser and Peltier cooled spray chamber. Analysis was conducted in normal sensitivity mode with detector attenuation employed for most m/z < 66 (Houk 1986). An external calibration approach was used. Standards and samples were all accurately spiked with a mixed internal standard stock solution to give 20 ppb lithium, 10 ppb scandium and 5 ppb yttrium, rhodium, indium, terbium, bismuth and thorium in all solutions. Internal standardisation was conducted using the instrument software interpolation function. The final concentrations were calculated from duplicate measurements and using the appropriate dilution factors, taking into account any variability in sensitivity and with errors calculated accordingly. The buffers used for the preparation of whole cell or organelle pellets i.e. DPBS, nuclei and mitochondria extraction buffers, were also analysed by ICP-MS. All samples were analysed as single samples, but each ICP-MS measurement was composed of five replicates.

Neutron activation analysis (NAA)—The elemental composition of the samples was determined by neutron activation analysis using the 20 MW OPAL research reactor (Bennett 2008). The k_0-method of standardisation (k_0-NAA) was used to maximise the number of elements that could be quantified. Certified reference material IRMM-530RC, produced by the Institute for Reference Materials and Measurements (IRMM), Geel, Belgium and containing 0.1% gold in aluminium, was used as the neutron flux monitor as well as the single comparator for k_0-NAA.

Since only a small amount (12–18 mg) of each sample was available for analysis, the usual method of splitting a sample into two aliquots to enable both a short (up to 15 minutes) and long (up to 20 hours) irradiation in OPAL could not be used. Instead, the samples were irradiated first in the long irradiation facility for 9 hours at a thermal neutron flux of 7×10^{12} cm^{-2} s^{-1} and, after being allowed to decay for four weeks, were subsequently irradiated in the short irradiation facility for between 1.5 and 2 minutes at a thermal neutron flux of 2.2×10^{13} cm^{-2} s^{-1}. After the long irradiation, multiple gamma-ray spectra were accumulated after decay periods ranging from 4 to 18 days. Analysis of these spectra using software

‡www.cbms.mq.edu.au

packages HyperLab and Kayzero for Windows enabled the concentration of sodium, potassium, iron, zinc, bromine, rubidium and lanthanum to be determined. After the short irradiation, spectra were accumulated after periods ranging from 2 to 18 minutes, enabling the concentration of magnesium, chlorine and manganese to be determined.

2.2. Monte Carlo Simulations

The elemental compositions derived from the experimental measurements were used in a Monte Carlo simulation study to determine the energy deposition and ionisation sensitivity of each sample. Two different cases were investigated: a homogeneous cell composed of a single material and a compartmentalised cell including the cell nucleus, cytosol and mitochondria volumes. The homogeneous cell case was used to isolate the physical effects resulting from the chemical composition, independent of the organelle geometry. The compartmentalised cell case was used to assess dose enhancement in the mitochondria and/or nucleus when gold is present in the cytosol.

Homogeneous cell—Four different spheres each with diameter 11.5 μm were modelled using the Monte Carlo simulation toolkit Geant4 v.10.01.p01 (Agostinelli et al. 2003, Allison et al. 2006). The diameter was chosen to match that of a typical T lymphocyte cell (Rosenbluth et al. 2006) and each spherical cell was submerged in a liquid water medium (i.e., modelled in suspension, see figure 1). Each cell was composed of a different chemical composition based on those derived from the experimental analysis for the whole cell, nucleus or mitochondrion. Since dry samples were required for the experimental chemical composition analysis, a percentage of liquid water (ranging from 10% to 100%) was added to each of the modelled dry biological materials. However, it was found that when irradiated by monoenergetic photons of energy 10 – 50 keV, cells consisting of 50 – 80% liquid water had approximately the same absorbed dose and total number of ionisation events, irrespective of the dry material used (whole cell, mitochondrion or nucleus). Since the average living human cell is estimated to consist of ~ 50 – 70% water, we present results only for the cellular materials consisting of 50% water and compare it to the 100% liquid water case. For all four cases, the density of the cell was set to 1 g cm^{-3}, equivalent to that of liquid water.

To determine the concentration of gold to add to the cell we referred to a recent study of GNP uptake in a mouse model (Wolfe et al. 2015). That study reported preferential whole tumour uptake from 10 mg/kg of GNP intravenous dose of 3–5 times the average body dose. This amounts to approximately 0.001% of gold in a whole tumour cell. However, it was also reported that the preparation resulted in higher intracellular uptake, with GNP clustering in the cytoplasm. This suggests that the GNP concentration in the cytoplasm would be significantly higher than 0.001%. Previous studies have also suggested that GNP concentrations of 0.05 – 1% can enhance dose in a cell (Cho 2005, Lechtman et al. 2011, McMahon et al. 2011*b*), thus we consider a mass percentage of 0.001% and 1% gold added to each of the biological materials.

Physical dose enhancement effects with gold have been shown to be more significant for keV energies rather than MeV photons (Lin et al. 2014, Cho 2005, Chithrani et al. 2010,

Lechtman et al. 2011) where the photoelectric effect dominates over Compton scatter. For this reason, a 12 × 12 μm^2 beam of incident monoenergetic photons with energies ranging from 10–50 keV was initiated at a distance of 10 μm from the centre of the cell (see figure 1). Monoenergetic beams were chosen to investigate the underlying physical processes involved in dose enhancement as a function of the photon energy. Each simulation run was repeated ten times with a different seed number and the final calculated values were averaged, with each run consisting of 10^8 parallel primary photons. The physical interactions within the cell volume were modelled with the Geant4 Low Energy Electromagnetic (EM) Package based on the Livermore libraries. The physical processes initialised for the incident photons included Compton scattering, Rayleigh scattering, the photoelectric effect and pair production. All secondary electrons were tracked and the physical processes activated for electrons included ionisation, bremsstrahlung and multiple scattering. The low energy cut-off for the production of secondary particles was set to 250 eV, the recommended lower limit of the physics package. Atomic deexcitation was activated including both fluorescence and the Auger effect. The production threshold of fluorescence and Auger electrons was disabled (i.e., no lower limit was set).

Compartmentalised Cell—A more realistic compartmentalised cell, containing the cell nucleus as well as mitochondria, was modelled with the Geant4 Low Energy Electromagnetic (EM) Package based on the Livermore libraries. The spherical cell had a diameter of 11.5 μm with a spherical nucleus of diameter 8.5 μm at the cell centre (Rosenbluth et al. 2006). Ellipsoid mitochondria with semi-axis lengths of 0.5 μm, 0.3 μm and 0.9 μm (Kam et al. 2013) were distributed in the cell volume outside the nucleus (see figure 2). The total mitochondrial volume was set to 11% of the total cell volume (Kam et al. 2013). The nucleus, cytosol and mitochondria were composed of the dry chemical compositions determined experimentally, taken with 50% liquid water. Gold (1% by mass) was added to the cytosol to investigate dose enhancement effects in the mitochondria and nucleus.

3. Results

The elemental composition was determined for a whole JURKAT cell as well as the isolated JURKAT cell nucleus and mitochondrion. These compositions were used in a Monte Carlo simulation study to investigate the ionisation susceptibility of different cell organelles relative to liquid water.

3.1. Experimental Results

Elemental composition of the JURKAT whole cell and organelles—The organic and inorganic compositions of the whole dry JURKAT cell are listed in Table 1 and represented in a bar graph in figure 3. All values are expressed as grams of element per 100 grams of sample. The elements shown are those detectable by each method, relative to the total mass of the sample. Some elements were undetectable e.g. oxygen and account for the missing mass in the tables. Carbon was the most abundant element detected in the whole cell, accounting for ~ 40% of the total mass of the sample. Other major inorganic salts detected were sodium (~ 3%), phosphorus (~ 2%), chlorine (~ 4%) and potassium (~ 2%).

Both ICP-MS and NAA quantified sodium, magnesium and rubidium in the whole cell sample with no significant difference between the values obtained by the two techniques. Rubidium behaves similarly to potassium in cells and has been found to occur in low concentrations (Relman 1956, Fieve et al. 1971), while molybdenum is known to play an important role in biological systems (Mendel & Bittner 2006). Lanthanum has no known function in cells but together with all other lanthanides was reported as < 0.01 ppm in the solution. Such low trace concentrations would have a negligible effect on the simulation results.

The organic and inorganic compositions of the dry JURKAT cell nucleus and mitochondrion are shown in Tables 2 and 3, respectively. In both organelles, carbon is again the most abundant element accounting for ~ 40% of the total mass. Due to the technical challenge of obtaining a sufficient amount of the material (~ 15 – 20 mg of dry organelle pellet) for NAA, ICP-MS was the only technique used to determine the inorganic component of each of the organelles. Chromium and nickel were found in both organelles but were not detected in the whole cell sample. The relative concentration of these two metals was likely too low in the whole cell sample to be detectable. However in the ”concentrated” organelle samples, these trace amounts are detectable.

Chlorine, potassium and copper were not found in the organelle samples, most likely due to the limited sensitivity of ICP-MS in the detection of these particular elements. However, it is highly likely that these elements would occur in these organelles (e.g. Pressman & Lardy 1955). The detection limits of ICP-MS depends on the analytes ionisation energy, abundance and background signal (for example, a high background due to polyatomic interfering species raises the detection limit). For some elements, detection is only possible at part per quadrillion (ppq) or part per trillion (ppt) levels. Quantitation limits (not only detected but quantified) are more conservative than detection limits (Houk 1994). Notably, the total percentage of measured trace metals (i.e., not carbon, hydrogen or nitrogen) in the nucleus and mitochondria were 3.6% and 4.2%, respectively.

A study investigating the light element composition (C, N and O) of rat hepatocyte cells found that carbon was the most abundant element in all three compartments, in agreement with our findings (Zierold et al. 2005). They also found that nitrogen was most abundant in the nucleus, however they report higher levels of nitrogen in the mitochondria than the cytoplasm, in disagreement with our findings. Another study investigating the elemental composition of rat hippocampal cells (Taylor et al. 1999), find higher levels of sodium in the cytoplasm and the mitochondria than the nucleus as well as similar amounts of calcium in all three components, in agreement with our findings. They also report on higher levels of magnesium in the nucleus, again in agreement with our results. With respect to the ICRU report 44 (ICRU 1989) data on the mass fraction of a cell nucleus, our results agree with the reported values of hydrogen (within ~ 6%), but disagree with the values obtained for carbon and nitrogen, which are both significantly lower than our results. Since the above investigations use different experimental techniques as well as different cell lines from our study, these deviations are not entirely unexpected.

3.2. Monte Carlo simulations

Homogeneous spherical cell—Potassium and chlorine were both absent from the experimental organelle materials due to the difficulty in obtaining a large enough sample for the chemical analysis. Even though our analysis was unable to detect potassium or chlorine, it is highly likely that they would occur in both organelles. In a test simulation we found that by excluding both elements from the whole cell composition, the energy deposition decreased by a factor of 1.6 and 1.44 for 10 and 35 keV incident photons, respectively. Since the presence of these elements have an effect on the results, both K and Cl were included in the organelle compositions with the same concentrations as that measured for the full cell case. There is evidence that both K and Cl concentrations in the nucleus are approximately the same as the rest of the cell (Palmer & Civan 1977). The potassium concentration varies within the mitochondrion depending on the activity of the cell but on average is similar to the concentration in the rest of the cell (Phillip et al. 2007). In addition, chlorine level in the mitochondria has also been reported to be approximately the same as the cell concentration within the reported error (Akar et al. 2003), thus we assume here that the concentrations are the same in both cellular components.

Table 4 summarises the material compositions used in the Monte Carlo simulation for the homogenous cell models. Table 4 also shows the mean ionisation energy for each modelled material as calculated by the Geant4 *G4 Material* class. Geant4 is unable to model realistic molecular bonds and treats all defined materials in terms of the proportion of individual elements, except for liquid water. Thus the mean ionisation energy of the material is based on that for individual elements. Table 4 shows that liquid water has the highest ionisation energy ($\simeq$ 78 eV) while the modelled mitochondrial composition has the lowest ($\simeq$ 68 eV). This suggests that the mitochondrial composition is the most ionisable of the materials modelled. Note that if water is modelled in Geant4 without bonds (i.e., defined as a material consisting of two hydrogen atoms and one oxygen atom instead of using the *G4 Water* material) it has an ionisation energy of $\simeq$ 69 eV. The mass attenuation coefficient μ/ρ for the whole cell composition was calculated to be ~ 6.6 cm^2/g from the mixture rule while that for the nucleus and mitochondria compositions was 6.7 cm^2/g and 7.4 cm^2/g, respectively, for 10 keV photons [§]. For comparison μ/ρ = 5.3 cm^2/g for 10 keV photons in water, lower than all the biological materials.

Figure 4 shows (a) the energy deposition and (b) total number of ionisations in each modelled material as a function of incident photon energy. Each measured composition is represented by the solid curves. The dashed curves show the case where a 1% mass fraction of gold was added to the material. The standard deviation for each point was less than 1%. A mass fraction of gold of 0.001% was also simulated for each case but the energy deposition increased by less than 0.2% for low photon energies and is not shown in this plot. At photon energies $\gtrsim$ 45 keV, both the number of ionisations and the energy deposition, irrespective of the material, is approximately the same as the liquid water case. At lower photon energies, however, differences between the biological materials and water are evident. This can be attributed to the photoelectric effect, which is the dominant photon interaction process at

[§]NIST: X-ray Mass Attenuation Coefficients

energies below about 30 keV. The biological materials respond differently to irradiation at low energies than liquid water, displaying both higher energy deposition and ionisation numbers. This demonstrates that simulations using liquid water as a surrogate for the cellular composition on small scales and at lower energies might not be realistic. All three biological materials however have similar properties, with the mitochondrial material displaying marginally higher energy deposition and ionisation numbers than the nucleus and whole cell materials.

Figure 4 also shows that adding 1% of gold increases both the energy deposition and the total number of ionisations for all the materials studied (dashed curves). The energy deposition in the whole cell material increases by a factor of 1.1, 2.1 and 1.7 for the gold case for 10, 30 and 50 keV incident photons, respectively. The mitochondria and nucleus materials both have an increase of ~ 2.0 for 30 keV photons. The increase observed for liquid water at 30 keV was a factor of 2.6, indicating that the use of liquid water in GNP simulations might not give an accurate estimate of dose enhancement effects. The trend for the total number of ionisations is similar to that for energy deposition for all three materials.

To confirm that photoelectrons and subsequent Auger cascades from the addition of gold contribute to short range electrons in the material, simulations were performed with and without the Auger processes activated in the whole cell material. We found that these processes increase the number of ionisations by a factor ~ 2.6. For the incident photon energies considered here, the L and M shell absorption edges of gold (E = 14.4 keV, 13.7 keV, 11.9 keV, 2.7 keV) are most likely to contribute to secondary Auger electron production. Furthermore, we investigated the increase in the photoelectric effect in the presence of gold. For the whole cell material, we find that adding 1% gold increases the occurrence of the photoelectric effect process by 14%.

Compartmentalised cell—Figure 5(a) shows the energy deposition and (b) total number of ionisations per unit volume in the cell nucleus and the mitochondria for the compartmentalised cell model as a function of incident photon energy. Results are shown for when 1% gold is added to the cytosol (dashed curves), compared to when no gold is added (solid curves). The presence of gold in the cytosol increases the energy deposited in both the mitochondria and nucleus volumes, however the overall increase is larger for the mitochondria (~ 32% averaged over all incident photon energies) than the nucleus (~ 13%).

The addition of 1% gold in the cytosol also increases the number of ionisations per unit volume for both organelles, with a larger effect observed for the mitochondria. The enhancement in energy deposition and number of ionisations in the organelles when 1% gold is added to the cytosol can be attributed to the delocalisation of energy on sub-micron scales by photoelectrons. The mean kinetic energy of photoelectrons created through a primary 10 keV photon interaction is ~ 3.8 keV, 4.1 keV and 4.3 keV for the whole cell, mitochondrion and nucleus materials, respectively. This corresponds to an average photoelectron range ~ 0.4 – 1 μm (also see Meesungnoen et al. 2002), implying that secondary electrons produced in the cytosol are capable of travelling to nearby organelles. Figure 6 shows a visualisation of a simulated photon track where the photoelectron produced in the cytosol delocalises to the mitochondrial volume. These results suggest that GNPs up-

taken into the cytosol can have a detrimental effect on the cell as a result of photoelectrons entering into nearby organelles, where they can cause damage that impairs important biological functions.

These results indicate that photoelectron delocalisation has a larger effect on mitochondria than the nucleus. The mitochondria occupy a smaller volume of the cell (11%) than the nucleus (40%) but are dispersed into many smaller volumes throughout the cell cytosol resulting in a larger surface area to volume ratio, 6.9 μm^{-1} compared to 0.7 μm^{-1} for the nucleus. The mitochondria thus have more surface area in direct contact with the cytosol than the nucleus and have more exposure to secondary electrons produced in the cytosol.

3.3. Discussion

To date the quantification of radiation damage has been largely focused on the DNA molecule but there may be other targets in a cell (Kuncic et al. 2012). Biological damage from the interaction of ionising radiation within biological tissue occurs when molecules are ionised and/or excited. In particular, low energy secondary electrons with energies less than ~ 1 keV typically produce more than ~ 50% of all ionisations, which may cause direct or indirect biological damage (Nikjoo & Goodhead 1991). All the simulations presented here were however restricted to a secondary electron cutoff of 250 eV and thus may underestimate the true number of ionisations generated in the materials. The Geant4-DNA (Very Low Energy) models (Incerti, Ivanchenko, Karamitros et al. 2010, Incerti, Baldacchino, Bernal et al. 2010, Karamitros et al. 2012) or other track structure algorithms (e.g. Friedland et al. 2011) are capable of modelling the discrete interactions of electrons down to the eV scale, a regime where a significant amount of excitation and ionisation processes occur (Munoz et al. 2012, Chauvie et al. 2006), but the Geant4-DNA package is currently restricted to a liquid water medium.

The simulations presented here assume an unrealistic uniform distribution of the elements, including gold, in the biological materials. Experimental studies have shown that GNPs cluster together in different regions of the cell (cytosol, lysosomes) and are unlikely to be uniformly distributed within cell or even within individual organelles (e.g. Chithrani et al. 2006, Peckys & de Jonge 2011). This could effect the distribution of energy deposition in the cell. It has however been demonstrated that GNPs may be attracted to the outer membrane of the mitochondrion (Karataş et al. 2009) or could be tagged to be up-taken by mitochondrion (Mkandawire et al. 2015). A recent Monte Carlo study showed that GNPs modelled on the membrane of mitochondria do indeed increase the overall dose received by the organelle (Kirkby & Ghasroddashti 2015). That study however did not consider realistic material compositions. Our results suggest that even if GNPs do not accumulate within the mitochondria, nanoparticles in close proximity to the organelle could still enhance damage due to the delocalisation of photoelectrons from the cytosol. Furthermore, a model that fully encapsulates the effects of radiation on the whole cell, not just the nuclear DNA, is essential for advancing our current understanding of the biological outcomes of irradiated cells (Waldren 2004, Baverstock & Belyakov 2005, Prise et al. 2005, McMahon et al. 2013, Byrne et al. 2013, Kuncic et al. 2012).

In practice therapeutic beams are polyenergetic, and even a high-energy spectra has a low-energy component which may trigger photoelectric effects. Furthermore, medium or high-energy radiation beams will interact with biological matter through the Compton effect, releasing lower energy photons which in turn can trigger photoelectric effects. Thus we can expect GNPs to enhance dose even for higher energy beams.

4. Conclusion

Our measurements of the chemical compositions for a whole human JURKAT cell, as well as its nucleus and mitochondrion revealed that the mitochondrial material had the highest mass attenuation coefficient (at < 30 keV) and lowest mean ionisation energy of all the materials studied. This suggests that mitochondria may be readily ionised when a cell is irradiated.

Additionally, we found that at low incident photon energies ($\lesssim$ 40 keV) both the absorbed dose and total number of ionisations generated in all the biological compositions differed significantly from that in liquid water. This suggests that using liquid water instead of realistic elemental compositions may produce less accurate results in Monte Carlo calculations of dose distributions and simulations of the physical mechanisms of radiation interactions of sub-cellular scales.

Using a more realistic compartmentalised cell model, we found that adding a 1% mass fraction of gold in the cytosol to represent nanoparticle uptake caused dose enhancement effects in both the nuclear and mitochondrial volumes. The physical mechanism responsible for this is photoelectron delocalisation from the cytosol to the organelles. This effect was found to be more prominent for the mitochondrial volume than the nuclear volume due to the larger surface area to volume ratio of the mitochondrion compared to the nucleus. From this we can conclude that even though gold nanoparticles tend to localise to the cytosol, physical dose enhancement effects are not restricted to the vicinity of the nanoparticles, but can extend to the nucleus and even more so to neighbouring mitochondria, thereby contributing to nanoparticle dose enhancement effects observed experimentally.

Acknowledgments

The authors acknowledge the Cancer Institute of NSW for funding the Advanced Computing Facility for Cancer Research which was used in this study. This work was in part supported by the National Institutes of Health (NIH)/ National Cancer Institute (NCI) grant R01 CA187003.

References

Agostinelli S, et al. Geant4 - a simulation toolkit. Nucl Instrum Methods A. 2003; 506(3):250–303.

Alard JP, Bodez V, Tchirkov A, Nénot ML, Arnold J, Crespin S, Rapp M, Verrelle P, Dionet C. Simulation of Neutron Interactions at the Single-Cell Level. Radiat Res. 2009; 158(5):650–656. [PubMed: 12385643]

Allison J, et al. Geant4 developments and applications. IEEE Trans Nucl Sci. 2006; 53(1):270–278.

Baverstock K, Belyakov OV. Classical radiation biology, the bystander effect and paradigms: a reply. Hum Exp Toxicol. 2005; 24(10):537–542. [PubMed: 16270755]

Bennett J. Commissioning of NAA at the new OPAL reactor in Australia. J Radioanal Nucl Ch. 2008; 278(3):671–673.

Byrne HL, Domanova W, McNamara AL, Incerti S, Kuncic Z. The cytoplasm as a radiation target: an in silico study of microbeam cell irradiation. Phys Med Biol. 2015; 60(6):2325–2337. [PubMed: 25715947]

Byrne H, McNamara A, Domanova W, Guatelli S, Kuncic Z. Radiation damage on sub-cellular scales: beyond DNA. Phys Med Biol. 2013; 58(5):1251. [PubMed: 23380838]

Cataldi A, Di Giacomo V, Rapino M, Zara S, Rana RA. Ionizing radiation induces apoptotic signal through protein kinase Cδ (delta) and survival signal through Akt and cyclic-nucleotide response element-binding protein (CREB) in Jurkat T cells. Biol Bull. 2009; 217(2):202–212. [PubMed: 19875824]

Champion C, Quinto MA, Monti JM, Galassi ME, Weck PF, Fojón OA, Hanssen J, Rivarola RD. Water versus DNA: new insights into proton track-structure modelling in radiobiology and radiotherapy. Phys Med Biol. 2015; 60(20):7805–7828. [PubMed: 26406277]

Chauvie S, Francis Z, Guatelli S, Incerti S, Mascialino B, Montarou G, Moretto P, Nieminen P, Pia MG, et al. Monte Carlo simulation of interactions of radiation with biological systems at the cellular and DNA levels: the Geant4-DNA project. Radiat Res. 2006; 166:676–677.

Chithrani BD, Ghazani AA, Chan WCW. Determining the Size and Shape Dependence of Gold Nanoparticle Uptake into Mammalian Cells. Nano Letters. 2006; 6(4):662–668. [PubMed: 16608261]

Chithrani DB, Jelveh S, Jalali F, van Prooijen M, Allen C, Bristow RG, Hill RP, Jaffray DA. Gold Nanoparticles as Radiation Sensitizers in Cancer Therapy. Radiat Res. 2010; 173(6):719–728. [PubMed: 20518651]

Cho SH. Estimation of tumour dose enhancement due to gold nanoparticles during typical radiation treatments: a preliminary Monte Carlo study. Phys Med Biol. 2005; 50(15):N163–N173. [PubMed: 16030374]

Fieve RR, Meltzer HL, Taylor RM. Rubidium chloride ingestion by volunteer subjects: Initial experience. Psychopharmacologia. 1971; 20(4):307–314. [PubMed: 5561654]

Friedland W, Dingfelder M, Kundrát P, Jacob P. Track structures, DNA targets and radiation effects in the biophysical Monte Carlo simulation code PARTRAC. Mutat Res-Fund Mol M. 2011; 711(1): 28–40.

Hainfeld JF, Slatkin DN, Smilowitz HM. The use of gold nanoparticles to enhance radiotherapy in mice. Phys Med Biol. 2004; 49(18):N309. [PubMed: 15509078]

Houk R. Mass spectrometry of inductively coupled plasmas. Anal Chem. 1986; 58(1):97A–105A.

Houk R. Elemental and isotopic analysis by inductively coupled plasma mass spectrometry. Acc Chem Res. 1994; 27(11):333–339.

ICRU. Tissue Substitutes in Radiation Dosimetry and Measurement. International Commission on Radiation Units and Measurements; 1989.

Incerti S, Baldacchino G, Bernal M, et al. The Geant4-DNA project. Int J Model Simul Sci Comput. 2010; 1(02):157–178.

Incerti S, Ivanchenko A, Karamitros M, et al. Comparison of GEANT4 very low energy cross section models with experimental data in water. Med Phys. 2010; 37(9):4692–4708. [PubMed: 20964188]

Joza N, Susin SA, Daugas E, Stanford WL, Cho SK, Li CY, Sasaki T, Elia AJ, Cheng HYM, Ravagnan L, et al. Essential role of the mitochondrial apoptosis-inducing factor in programmed cell death. Nature. 2001; 410(6828):549–554. [PubMed: 11279485]

Kam WWY, Banati RB. Effects of ionizing radiation on mitochondria. Free Radical Bio Med. 2013; 65:607–619. [PubMed: 23892359]

Kam WWY, McNamara AL, Lake V, Banos C, Davies JB, Kuncic Z, Banati RB. Predicted ionisation in mitochondria and observed acute changes in the mitochondrial transcriptome after gamma irradiation: A Monte Carlo simulation and quantitative PCR study. Mitochondrion. 2013; 13(6): 736–742. [PubMed: 23485772]

Karamitros M, Incerti S, Champion C. The Geant4-DNA project. Radiother Oncol. 2012; 102:S191–S192.

Karataş ÖF, Sezgin E, Aydın Ö, Çulha M. Interaction of gold nanoparticles with mitochondria. Colloids and Surfaces B. 2009; 71(2):315–318.

Kirkby C, Ghasroddashti E. Targeting mitochondria in cancer cells using gold nanoparticle-enhanced radiotherapy: A Monte Carlo study. Med Phys. 2015; 42(2):1119–1128. [PubMed: 25652523]

Kuncic Z. Advances in computational radiation biophysics for cancer therapy: simulating nano-scale damage by low-energy electrons. Biophysical Reviews and Letters. 2015; 10(1):25–36.

Kuncic Z, Byrne HL, McNamara AL, Guatelli S, Domanova W, Incerti S. In silico nanodosimetry: New insights into nontargeted biological responses to radiation. Comput Math Methods Med. 2012; 2012:1–9.

Larsen N, Rasmussen M, Rasmussen L. Nuclear and mitochondrial DNA repair: Similar pathways? Mitochondrion. 2005; 5(2):89–108. [PubMed: 16050976]

Lechtman E, Chattopadhyay N, Cai Z, Mashouf S, Reilly R, Pignol JP. Implications on clinical scenario of gold nanoparticle radiosensitization in regards to photon energy, nanoparticle size, concentration and location. Phys Med Biol. 2011; 56(15):4631–4647. [PubMed: 21734337]

Lin Y, McMahon SJ, Scarpelli M, Paganetti H, Schuemann J. Comparing gold nano-particle enhanced radiotherapy with protons, megavoltage photons and kilovoltage photons: a Monte Carlo simulation. Phys Med Biol. 2014; 59(24):7675–7689. [PubMed: 25415297]

McBride HM, Neuspiel M, Wasiak S. Mitochondria: more than just a powerhouse. Curr Biol. 2006; 16(14):R551–R560. [PubMed: 16860735]

McMahon SJ, Butterworth KT, Trainor C, McGarry CK, O'Sullivan JM, Schettino G, Hounsell AR, Prise KM. A kinetic-based model of radiation-induced intercellular signalling. PloS ONE. 2013; 8(1):e54526. [PubMed: 23349919]

McMahon SJ, Hyland WB, Muir MF, Coulter JA, Jain S, Butterworth KT, Schettino G, Dickson GR, Hounsell AR, O'Sullivan JM, Prise KM, Hirst DG, Currell FJ. Biological consequences of nanoscale energy deposition near irradiated heavy atom nanoparticles. Scientific Reports. 2011a:1. [PubMed: 22355520]

McMahon SJ, Hyland WB, Muir MF, Coulter JA, Jain S, Butterworth KT, Schettino G, Dickson GR, Hounsell AR, O'Sullivan JM, Prise KM, Hirst DG, Currell FJ. Nanodosimetric effects of gold nanoparticles in megavoltage radiation therapy. Radiother Oncol. 2011b; 100(3):412–416. [PubMed: 21924786]

Meesungnoen J, Jay-Gerin JP, Filali-Mouhim A. Low-energy electron penetration range in liquid water. Radiat Res. 2002; 158(5):657–660. [PubMed: 12385644]

Mendel RR, Bittner F. Cell biology of molybdenum. BBA-Mol Cell Res. 2006; 1763(7):621–635.

Mkandawire MM, Lakatos M, Springer A, Clemens A, Appelhans D, Krause-Buchholz U, Pompe W, Rödel G, Mkandawire M. Induction of apoptosis in human cancer cells by targeting mitochondria with gold nanoparticles. Nanoscale. 2015; 7(24):10634–10640. [PubMed: 26022234]

Munoz, A.; Fuss, MC.; Cortés-Giraldo, M.; Incerti, S.; Ivanchenko, V.; Ivanchenko, A.; Quesada, J.; Salvat, F.; Champion, C.; Gómez-Tejedor, GG. Radiation Damage in Biomolecular Systems. Springer; 2012. p. 203-225.

Murphy JE, Nugent S, Seymour C, Mothersill C. Mitochondrial DNA point mutations and a novel deletion induced by direct low-LET radiation and by medium from irradiated cells. Mutat Res-Gen Tox En. 2005; 585(1):127–136.

Nicholls DG, Chalmers S. The integration of mitochondrial calcium transport and storage. J Bioenerg Biomembr. 2004; 36(4):277–281. [PubMed: 15377857]

Nikjoo H, Goodhead D. Track structure analysis illustrating the prominent role of low-energy electrons in radiobiological effects of low-LET radiations. Phys Med Biol. 1991; 36(2):229. [PubMed: 2008448]

Palmer LG, Civan MM. Distribution of Na+, K+ and Cl- between nucleus and cytoplasm in Chironomus salivary gland cells. J Membrane Biol. 1977; 33(1):41–61. [PubMed: 864686]

Peckys DB, de Jonge N. Visualizing Gold Nanoparticle Uptake in Live Cells with Liquid Scanning Transmission Electron Microscopy. Nano Letters. 2011; 11(4):1733–1738. [PubMed: 21410218]

Phillip, S.; Downey, JM.; Cohen, MV. Mitochondria. Springer New York; New York, NY: 2007. p. 305-322.

Pressman BC, Lardy HA. Further studies on the potassium requirements of mitochondria. Biochim Biophys Acta. 1955; 18(0):482–487. [PubMed: 13304029]

Prise KM, Schettino G, Folkard M, Held KD. New insights on cell death from radiation exposure. Lancet Oncol. 2005; 6(7):520–528. [PubMed: 15992701]

Prithivirajsingh S, Story MD, Bergh SA, Geara FB, Kian Ang K, Ismail SM, Stevens CW, Buchholz TA, Brock WA. Accumulation of the common mitochondrial DNA deletion induced by ionizing radiation. FEBS letters. 2004; 571(1):227–232. [PubMed: 15280047]

Raimundo N. Mitochondrial pathology: stress signals from the energy factory. Trends Mol Med. 2014; 20(5):282–292. [PubMed: 24508276]

Relman AS. The physiological behavior of rubidium and cesium in relation to that of potassium. Yale J Biol Med. 1956; 29(3):248–262. [PubMed: 13409924]

Rosenbluth MJ, Lam WA, Fletcher DA. Force microscopy of nonadherent cells: a comparison of leukemia cell deformability. Biophys J. 2006; 90(8):2994–3003. [PubMed: 16443660]

Taggart LE, McMahon SJ, Currell FJ, Prise KM, Butterworth KT. The role of mitochondrial function in gold nanoparticle mediated radiosensitisation. Cancer Nanotechnology. 2014; 5(1):1–12. [PubMed: 26561509]

Taylor CP, Weber ML, Gaughan CL, Lehning EJ, LoPachin RM. Oxygen/glucose deprivation in hippocampal slices: altered intraneuronal elemental composition predicts structural and functional damage. J Neurosci. 1999; 19(2):619–629. [PubMed: 9880582]

Thiers RE, Vallee BL. Distribution of metals in subcellular fractions of rat liver. J Biol Chem. 1957; 226(2):911–920. [PubMed: 13438880]

Waldren CA. Classical radiation biology dogma, bystander effects and paradigm shifts. Hum Exp Toxicol. 2004; 23(2):95–100. [PubMed: 15070068]

Wolfe T, Chatterjee D, Lee J, Grant JD, Bhattarai S, Tailor R, Goodrich G, Nicolucci P, Krishnan S. Targeted gold nanoparticles enhance sensitization of prostate tumors to megavoltage radiation therapy in vivo. Nanomedicine: Nanotechnology, Biology and Medicine. 2015; 11(5):1277–1283.

Woodard HQ, White DR. The composition of body tissues. Brit J Radiol. 1986; 59(708):1209–1218. [PubMed: 3801800]

Zhang B, Davidson MM, Hei TK. Mitochondria regulate DNA damage and genomic instability induced by high LET radiation. Life Sciences in Space Research. 2014; 1:80–88. [PubMed: 25072018]

Zhang SB, Maguire D, Zhang M, Zhang Z, Zhang A, Yin L, Zhang L, Huang L, Vidyasagar S, Swarts S, et al. The murine common deletion: Mitochondrial DNA 3,860-bp deletion after irradiation. Radiat Res. 2013; 180(4):407–413. [PubMed: 24059680]

Zierold K, Michel J, Terryn C, Balossier G. The Distribution of Light Elements in Biological Cells Measured by Electron Probe X-Ray Microanalysis of Cryosections. Microsc Microanal. 2005; 11(02):138–145. [PubMed: 15817143]

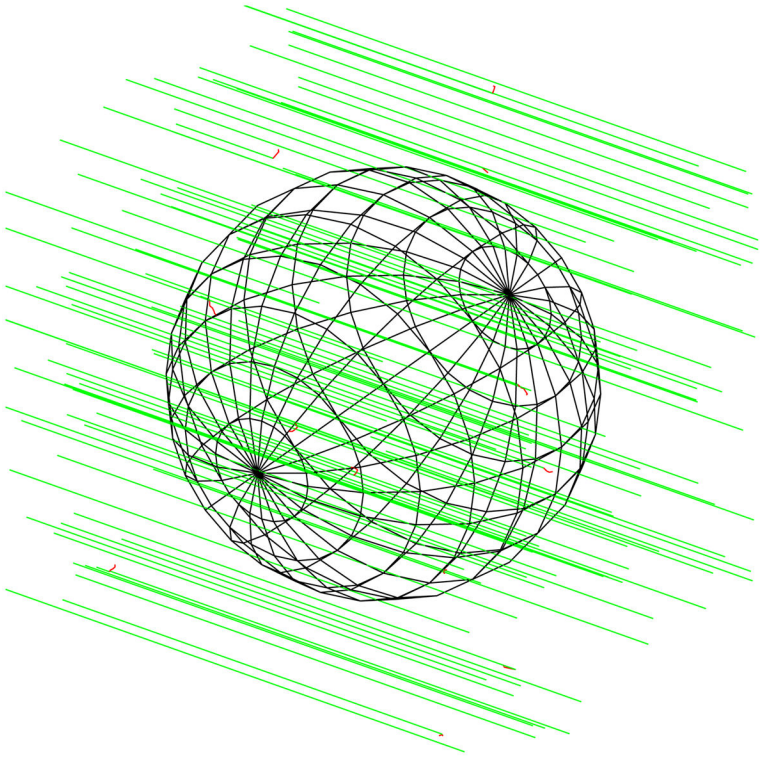

Figure 1.
Schematic illustration of the homogeneous spherical cell model of diameter 11.5 μm, suspended in liquid water. A broad beam of monoenergetic incident photons emitted at a distance of 10 μm from the cell centre is shown in green. Secondary electron tracks are shown in red.

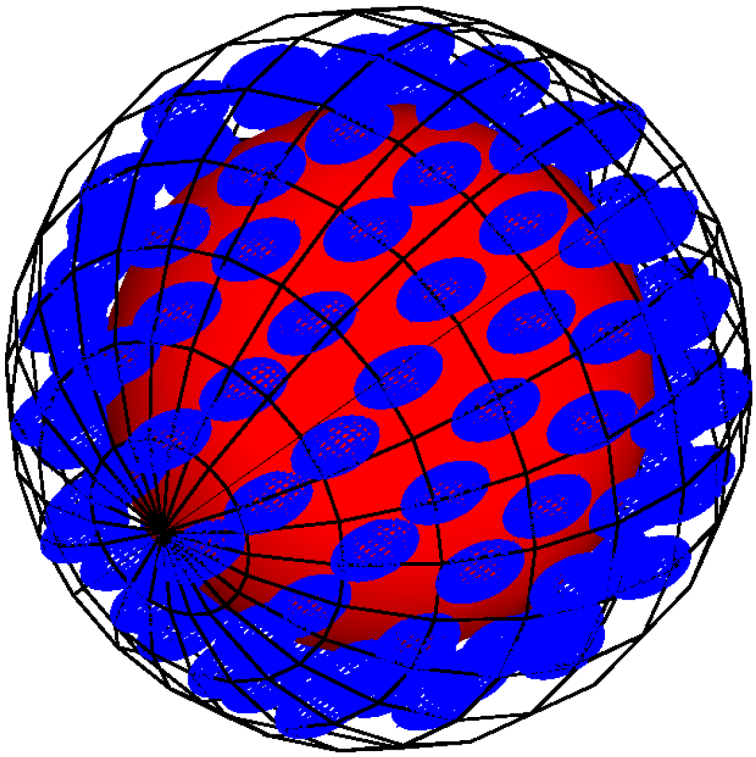

Figure 2.
Schematic illustration of the compartmentalised cell model. The model included a centrally located spherical nucleus (red) and ellipsoid mitochondria (blue) distributed throughout the cytosol. The cell was suspended in liquid water and irradiated with a broad beam of incident photons, emitted at a distance of 10 μm from the cell centre. Gold was added to the cytosol to investigate possible dose enhancement effects in the organelle volumes.

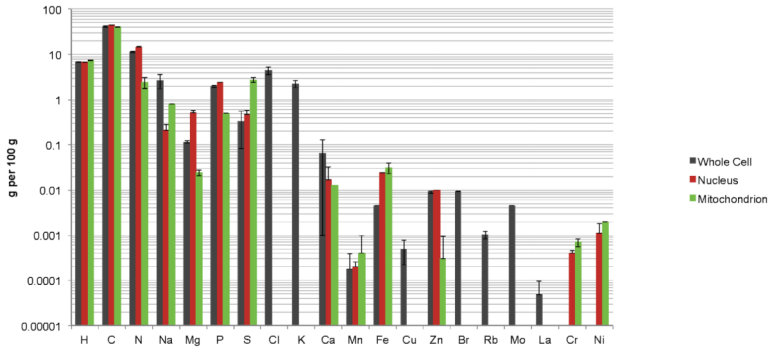

Figure 3.

Bar graph showing the relative chemical concentrations determined experimentally for the JURKAT whole cell (grey), cell nucleus (red) and mitochondrion (green) dry samples. Cl, K, Br and La were detected using NAA, a technique only available for the whole cell material due to sample size constraints.

(a)

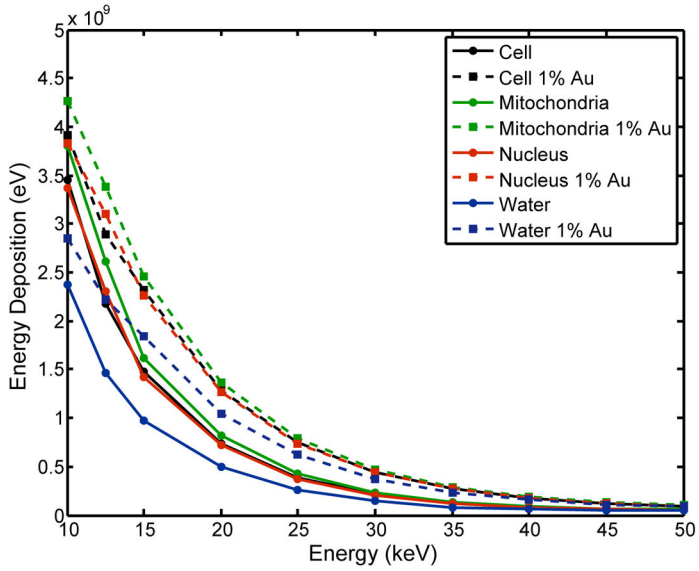

(b)

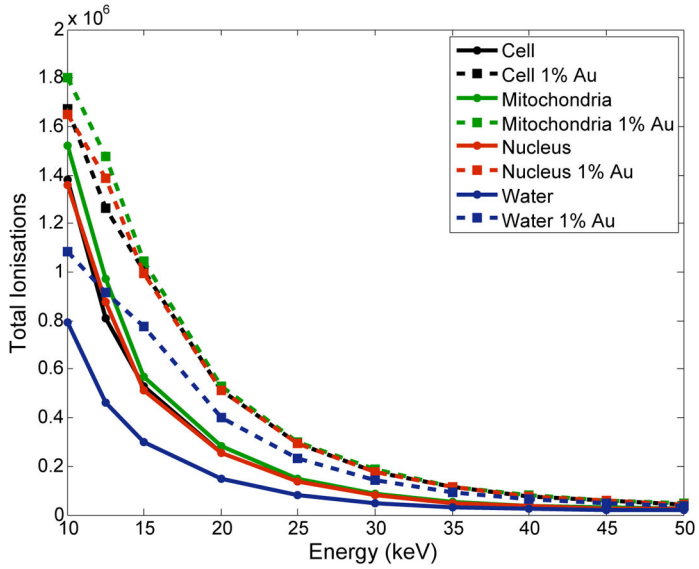

Figure 4.

(a) Monte Carlo calculated energy deposition and (b) total number of ionisations as a function of photon energy, in a homogeneous cell of diameter 11.5 μm consisting of different biological materials. In each case, the chemical composition consisted of 50% of the dried measured sample composition and 50% liquid water. The solid curves represent the material without gold, while the dashed lines represent the material with 1% mass fraction of gold.

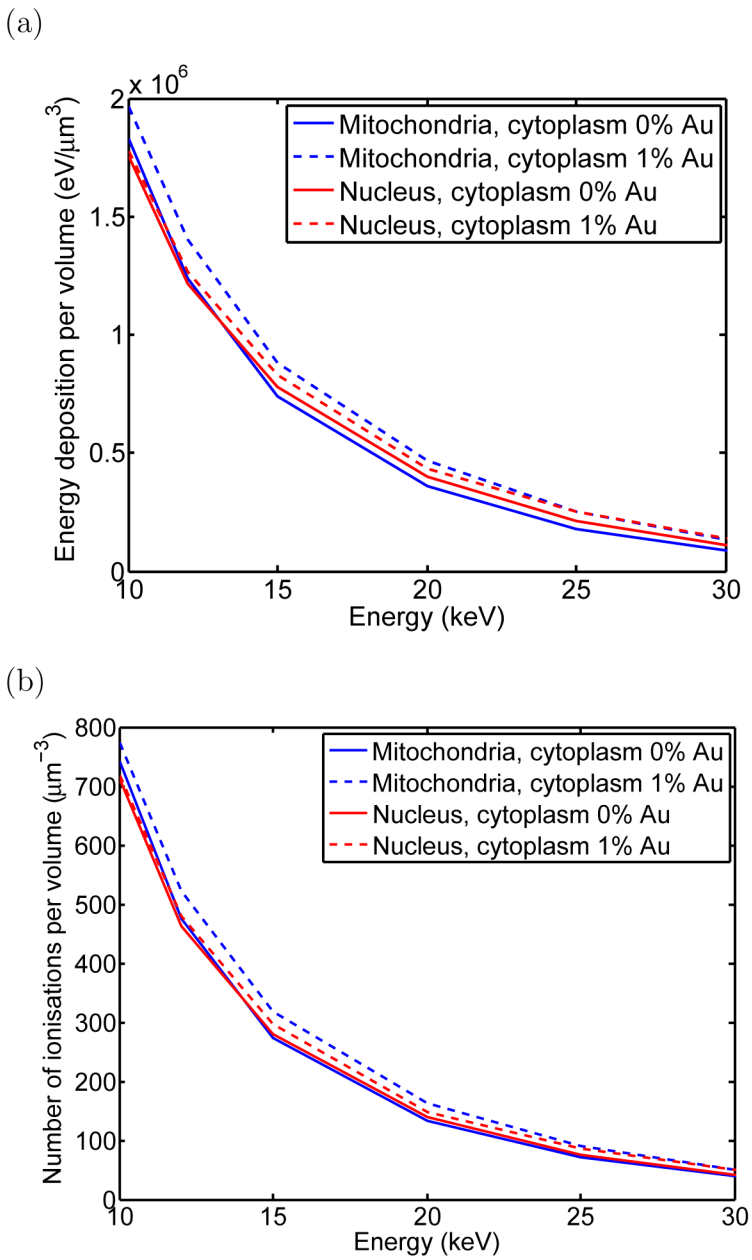

Figure 5.

(a) The energy deposition per unit volume in the nucleus (red) and the mitochondria (blue) in a modelled compartmentalised cell when the cytosol contains 1% gold (dashed curves) compared to the case where the cytosol does not contain gold (solid curves) as a function of incident photon energy. (b) The total number of ionisations per unit volume in the nucleus and the mitochondria in a modelled compartmentalised cell when the cytosol contains 1% gold compared to the case where the cytosol does not contain gold as a function of incident photon energy.

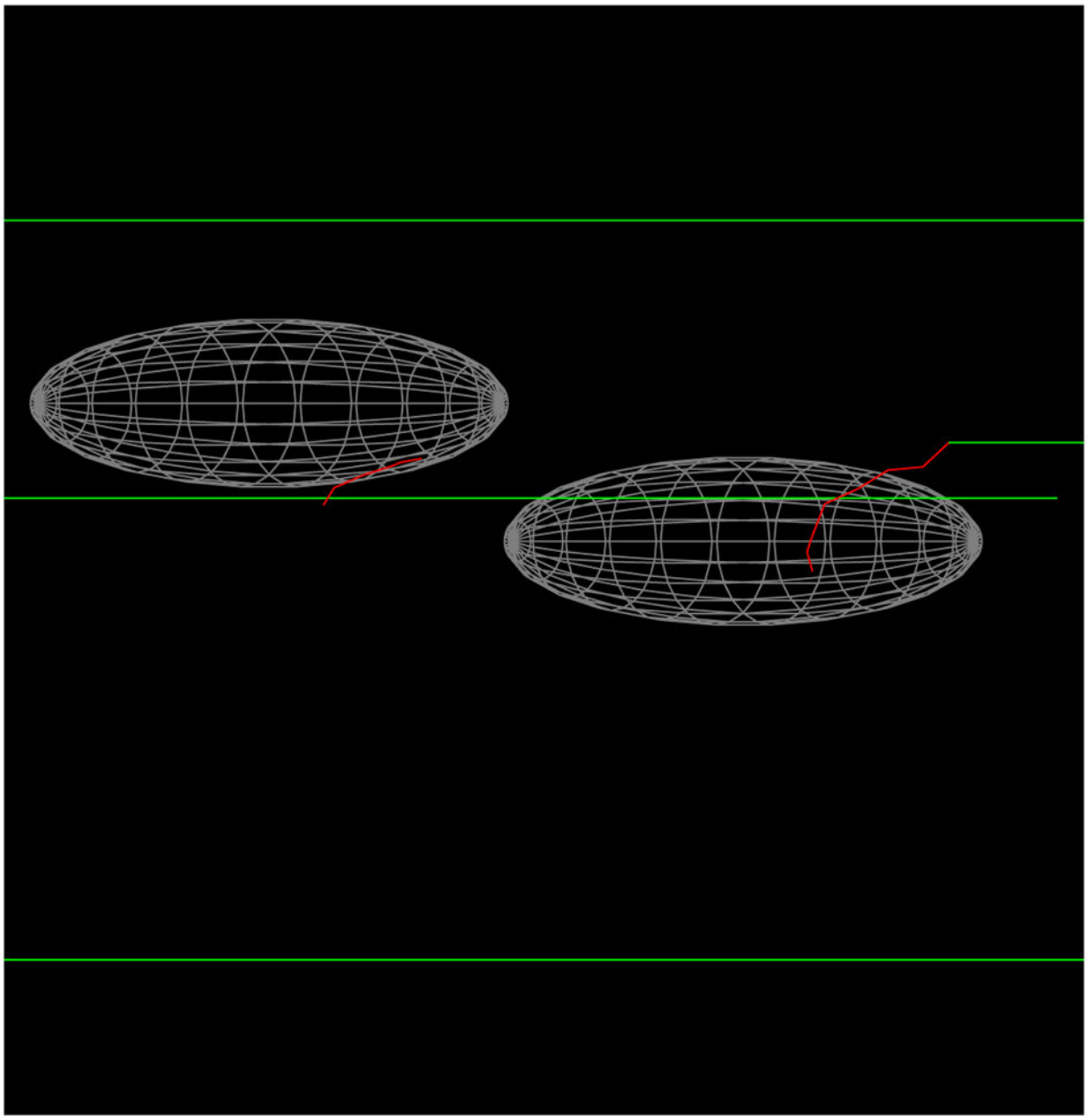

Figure 6.
Illustration of the simulated 10 keV incident photons (green) interacting with mitochondria in the compartmentalised cell model. A secondary photoelectron (red) is produced in the cytosol but delocalises to the mitochondrial volume.

Table 1

Elemental composition of a dry mammalian JURKAT cell analysed by CHNS analysis, ICP-MS and NAA. Values are expressed as grams of element per 100 grams of sample. The standard deviation (SD) indicates the variation between biological replicates. Two elements, Mo (by ICP-MS) and Fe (NAA), could only be detected in one sample among those analysed.

		CHNS (N=3)		ICP-MS (N=2)		NAA (N=4)	
Element	**A**	**Average**	**SD**	**Average**	**SD**	**Average**	**SD**
H	1	6.77	0.13				
C	6	41.48	1.63				
N	7	11.32	0.26				
Na	11			2.65	0.92	3.2	0.7
Mg	12			0.1150	0.0071	0.11	0.01
P	15			1.950	0.071		
S	16	0.32	0.24				
Cl	17					4.4	0.8
K	19					2.2	0.4
Ca	20			0.065	0.064		
Mn	25					0.0002	0.0002
Fe	26					0.0002	–
Cu	29			0.00050	0.00028		
Zn	30			0.00905	0.00064	0.0090	0.0003
Br	35					0.0008	0.0003
Rb	37			0.00102	0.00011	0.0010	0.0002
Mo	42			0.00045	–		
La	57					0.00005	0.00005

Table 2

Elemental composition of a dry mammalian JURKAT cell nucleus analysed by CHNS analysis, ICP-MS and NAA. Values are expressed as grams of element per 100 grams of sample. SD indicates the variation between biological replicates.

		CHNS (N=3)		ICP-MS (N=2)	
Element	**A**	**Average**	**SD**	**Average**	**SD**
H	1	6.61	0.15		
C	6	44.21	0.45		
N	7	14.56	0.76		
Na	11			0.210	0.070
Mg	12			0.51	0.076
P	15			2.4	–
S	16	0.47	0.10		
Ca	20			0.017	0.016
Cr	24			0.000400	0.000058
Mn	25			0.000200	0.000058
Fe	26			0.02400	0.00058
Ni	28			0.00110	0.00072
Zn	30			0.01	–

Table 3

Elemental composition of a dry mammalian JURKAT cell mitochondrion analysed by CHNS analysis, ICP-MS and NAA. Values are expressed as grams of element per 100 grams of sample. SD indicates the variation between biological replicates.

		CHNS (N=3)		ICP-MS (N=2)	
Element	**A**	**Average**	**SD**	**Average**	**SD**
H	1	7.450	0.073		
C	6	40.78	0.96		
N	7	2.43	0.67		
Na	11			0.81	0.01
Mg	12			0.0240	0.0035
P	15			0.5	–
S	16	2.77	0.36		
Ca	20			0.013	–
Cr	24			0.00070	0.00015
Mn	25			0.000400	0.000058
Fe	26			0.0310	0.0081
Ni	28			0.002	–
Zn	30			0.00030	0.00064

Table 4

Elemental mass fraction (%) of the compositions used in the Monte Carlo homogeneous cell simulation for the whole cell, nucleus and mitochondrion materials. Elements with mass fractions less than 0.01% have negligible effects on the simulations and is thus not included. All material densities were assumed to be 1 g/cm^3. For comparison, the elemental composition of liquid water is included.

Element	Liquid water*	Whole cell	Nucleus	Mitochondria
H	11.19	10.34	9.96	11.65
C		29.08	29.22	33.19
N		7.94	9.62	1.98
O	88.81	44.41	44.41	44.41
Na		1.86	0.14	0.66
Mg		0.08	0.34	0.02
P		1.37	1.59	0.41
S		0.23	0.31	2.25
Cl		3.08	2.91	3.58
K		1.55	1.46	1.80
Ca		0.05	0.01	0.01
Fe		0.00	0.02	0.03
Zn		0.01	0.01	0.00
Br		0.01	-	-
Mean Ionisation Energy	78.00 eV	69.76 eV	69.91 eV	67.97 eV

* Defined from the Geant4 NIST database